Optical and Quantum Electronics (2023) 55:793
https://doi.org/10.1007/s11082-023-05055-6

Design of 1-to-2-line all-optical decoder based on MMI phase shifter

Kamanashis Goswami[1] · Haraprasad Mondal[1,2] · Mrinal Sen[1]

Received: 23 February 2023 / Accepted: 7 June 2023

Abstract
Design of an all-optical 1:2 decoder has been proposed based on a holes-in-slab photonic crystal structure. Operation of the device depends on optical interferometry of an input and a bias signal. In order to achieve wavelength independent optical interference, a multimode Interference (MMI) based π-phase shifter is proposed, analysed and integrated within the design of the decoder. Dispersion diagram of the MMI π-phase shifter depicts almost equal slope of two propagation bands for a long range of wavelengths, which ensures its wavelength insensitive phase-shift operation. Finite Difference Time Domain (FDTD) simulation also confirms the same. Further, several simulations and corresponding analyses for evaluating different performances of the decoder have also been performed. These analyses exhibit the successful decoding operation of the device. The decoder performance has also been studied under the excitation of pulsating input and bias. This study concludes that the device is able to process a bit-rate as-high-as 2.94 Tbps. This small footprint (~243 μm^2) device also offers an excellent contrast ratio of the order of 20 dB. Hence, it is expected that the device would be a potential candidate for implementing complex circuitries in photonic integrated circuits.

Keywords Optical decoder · Photonic crystal · Beam interference · Phase shifter · Band diagram

✉ Mrinal Sen
mrinal.sen.ahm@gmail.com

Kamanashis Goswami
kamanashis.goswami@gmail.com

Haraprasad Mondal
mandal.haraprasad@gmail.com

[1] Electronics Engineering, Indian Institute of Technology (ISM) Dhanbad, Dhanbad, Jharkhand, India

[2] Dibrugarh University Institute of Engineering and Technology, Dibrugarh University, Dibrugarh, Assam 786001, India

Published online: 30 June 2023

1 Introduction

In spite of continual incremental progress in VLSI technology, the conventional electronic circuitry is gradually failing to keep pace with human race's evolving demand for high-speed data processing. Contextually, a large cluster of researchers and technology providers believes that now Electronics needs to pass on the flag of this relay race to Optics to maintain the pace. Optics, especially the all-optical Photonic Integrated Circuits (PICs) (Yablonovitch 1987; Baqir et al. 2018; Alipore et al. 2018), facilitated by interesting optical properties of silicon and its mature fabrication processes, has already kicked off the race by producing several high-performance devices over the last two decades. It has also improved the communication system by providing high bandwidth transceivers, and avoiding the need for optical to electrical, and vice versa, conversion in repeater nodes. However, to win the race, it also needs to alleviate the data rate bottlenecking in electronic processing. In consequence, optical Boolean logic devices, like—gates (Goswami et al. 2022; Fu et al. 2013; Lin et al. 2013; Mondal et al. 2022, 2015), decoder/encoder (Lee et al. 2006; Cabezón et al. 2014; Kim 2000; Chen et al. 2006; Chung et al. 2006; Sharma et al. 2022), multiplexer/demultiplexer (Moniema 2015; Mondal et al. 2019, 2018a; Gogoi et al. 2016; Zhu and Li 2006), adder/subtractor (Jiu-Sheng et al. 2015; Xie et al. 2017), becomes inevitable to design data processing/computation units in optical domain. Further, in the discussion of designing-platforms for all-optical logic devices; especially for PICs, the first name appears in one's mind is the Photonic Crystal (PhC) (Goswami et al. 2020a, 2020b, 2022a; Prakash et al. 2018a, 2018b). The PhC has earned this popularity as it is equipped with several important properties like – photonic band gap (PBG) (Joannopoulos et al. 2008), self-collimation (Sukhoivanov and Guryev 2009), slow-light propagation, and comparatively easy manipulation of light propagation than that in other platforms. In the recent past, several all-optical logic devices have been designed by enriching different optical phenomena, like—interference (Chen et al. 2006; Liu et al. 2013) and nonlinearity (Mehdizadeh et al. 2018; Rostami 2007; Sahoo and Joseph 2013; Zhao et al. 2019), utilizing these interesting properties of PhC. Among the different all-optical logic devices, the all-optical decoder (AOD) is an important device for designing PIC based computational units and other complex logic circuits. Hence, a number of researchers have proposed PhC based AODs utilizing linear as well as nonlinear optical phenomena. For example, a nonlinear ring-resonator designed in the PhC platform (PhCNRR) has been used by Serajmohammadi et al. (2019) to model a 1-to-2 line AOD within a footprint of 238 μm^2. Similarly, Askarian (2021) has used two PhCNRRs to design a 2-to-4-line AOD, having a footprint of 420 μm^2, utilizing beam interference and threshold switching. Some 2-to-4-line AODs have also been proposed in (Alipour-Banaei et al. 2015; Khosravi and Zavvari 2018; Maleki et al. 2019) using multiple PhCNRRs. Likewise, Salimzadeh and Alipour-Banaei (2018) has combined seven number of PhCNRR based 1-to-2 line AODs to design a 3-to-8 line AOD. However, these AODs, like other optical nonlinearity-based devices, suffers from the unavoidable limitation of threshold power that prohibits their operation below a certain optical input power. Keeping this in mind, several research works (Haraprasad mondal et al. 2019; Mondal et al. 2016, 2018b) have utilized only linear optical phenomena, especially the beam interference, to design PhC based AODs. For example, Alipour-Banaei et al. (2015) have used three PhC ring-resonators (PhCRRs) to design a 2-to-4-line decoder on a 29×22 square array of chalcogenide glass rods utilizing the self-collimation and interference phenomena. Similarly, multiple PhCRRs and interference in PhCWs/ PhC-cavities have been used to design 2-to-4-line decoders in (Mehdizadeh et al.

2016, 2017, 2018). However, most of these PhC based linear AODs are designed using 2D rods-in-air PhC structure, which is mechanically fragile (Joannopoulos et al. 2008; Johnson et al. 1999). Also, majority of these designs have neither considered a 3D structure nor the 2D effective-index, for which their simulated outcomes are expected to deviate significantly from the experimental ones. Additionally, most of the reported designs offer bit rates in Gbps range. Moreover, the optical interference phenomenon is strongly dependent on the phase difference of the input optical beams, which again is dependent on the wavelength of the input waves as the propagation constant is usually a function of the wavelength. This factor in most of the above cases limits the performance of the interference based linear optical devices within the designated wavelength. Further, the design needs to be analysed using either the highly computationally intensive 3D simulation (having high accuracy) or the computationally less-intensive 2D effective-index simulation (having lower accuracy than the former) methods to obtain reliable outcomes.

Thereby, the paper, at first, proposes the design of a (holes-in-slab) PhC based MMI structure to introduce wavelength insensitive π-phase shift to an incoming wave. The phase shifter is designed based on the dispersion characteristics of a W3 PhC, calculated using the Plane Wave Expansion (PWE) (Johnson and Joannopoulos 2001; https://mpb.readthedocs.io/en/latest/Introduction/ 2023) method. As stated before, such a structure is quite important for designing interferometry-based devices, but, as per the authors' best knowledge, has not been reported earlier in the literature. Thereafter, the phase-shifter is used to design a PhC based AOD utilizing interference and other linear optical phenomena. Performances of the phase-shifter and the AOD have been evaluated using the 2D Finite Difference Time Domain (FDTD) (Huang et al. 1991; https://www.synopsys.com/photonic-solutions/rsoft-photonic-device-tools/passive-devicefullwave.html 2023) method considering the effective index of the slab to produce outcomes which are reasonably close to its 3D counterpart. Moreover, to execute the FDTD simulation process the parameters like time step, grid spacing, and boundary conditions have been taken as 0.0466 fs, Dx = 28 nm Dy = 14 nm Dz = 390 nm and boundary condition = PML (perfectly matched layer) respectively. The results show that the AOD assimilates the behaviour of a Boolean logic decoder based on optical power and can support a high bit-rate operation in the range of Tbps. Further detailing of the device and corresponding analyses are given in the successive sections, which has been followed by an overall conclusion on the work.

2 Device model

The design of the decoder is based on the interference of two optical waves with the same wavelength. While interference-based devices work efficiently at the designated wavelength and appear easy to design, their performance suffers at wavelengths other than the designated one. This is because the propagation constant varies across wavelengths, and the waveguide length does not produce the required phase-shift for successful device operation at all wavelengths. To address this issue, a phase shifter that generates a fixed phase-shift for a range of wavelengths can be designed. However, such a device is challenging to design and is crucial for the successful operation of interferometer-based logic devices. Therefore, the first phase of the device modeling

proposes the design of a wavelength-insensitive/independent phase shifter, which is elaborated in the following subsection.

2.1 A wavelength independent π-phase-shifter

The design of the proposed phase shifter relies on the principle of self-imaging, which occurs within a multi-mode interference (MMI) structure. The MMI structure is modeled using a W3 photonic crystal (PhC) waveguide. In this design, the PhC consists of a silicon slab with air-hole perforations, and the arrangement of these holes forms a periodic triangular lattice with a lattice constant 'a'. The radius of the air-holes is set to 0.32a. Refractive index of the silicon is considered here as 3.46, and the height of the slab is taken as 0.7a to attain a large band-gap of the PhC (Sukhoivanov and Guryev 2009). Applying plane wave expansion (PWE) algorithm the complete photonic

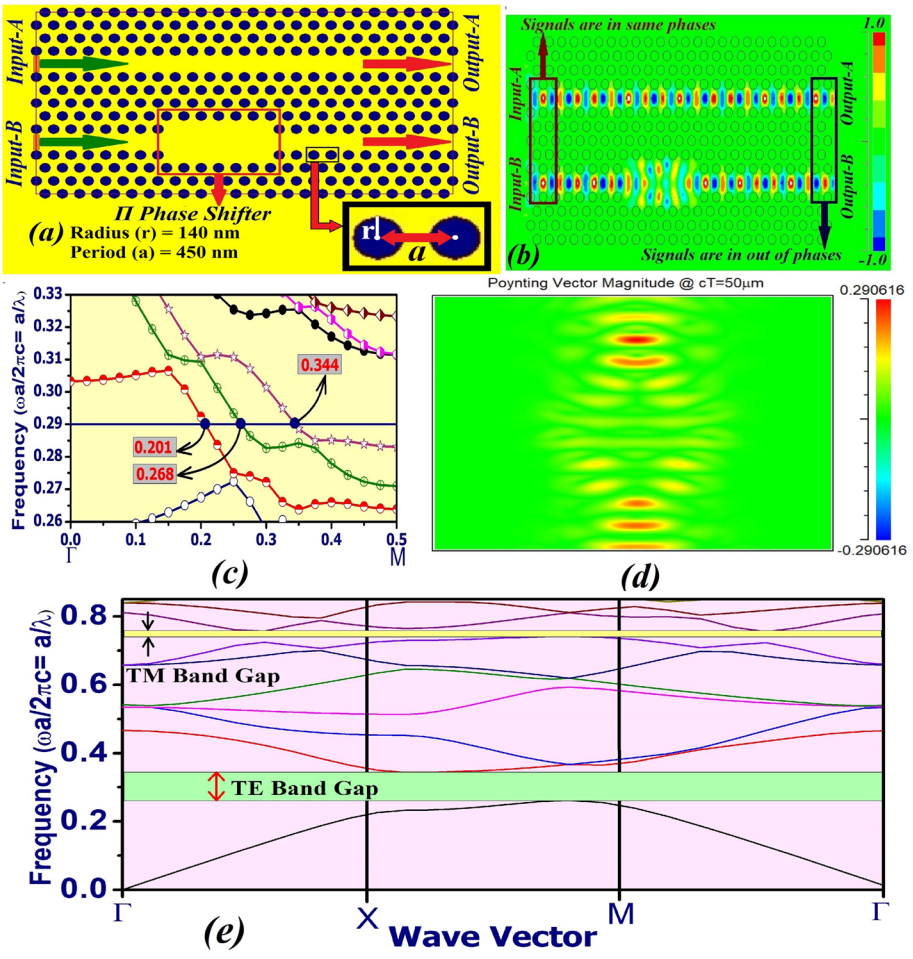

Fig. 1 **a** Physical model of π phase shifter **b** field propagation through π phase shifter **c** dispersion diagram for waveguide **d** higher modes in W3 waveguide **e** Complete photonic band gap of PhC structure

band gap of the PhC structure in both transverse electric (TE) and transverse magnetic (TM) modes has been calculated, which is shown in Fig. 1e. From Fig. 1e, it has been observed that band gap obtained in the range of normalized frequency 0.25 to 0.34 (in wave length equivalent of 1320 nm to 1800 nm) in TE mode whereas, an extremely narrow band gap in the normalized frequency range of 0.74 to 0.76 (in wave length equivalent of 592 nm to 608 nm) has been obtained in TM mode. However, Fig. 1a illustrates the physical model of the phase shifter. As depicted in the figure, the input signal can be introduced to the W3 PhC waveguide-based phase shifter from the left side through a port based on the W1 PhC waveguide. The wave travels through this 7a long MMI device and originates a self-image at the output port (the W1 PhC waveguide at the right-side of the structure), however with a π phase-shift than that would have appeared in a 7a long W1 PhC waveguide. To illustrate the wave propagation operation through the device, a Finite Difference Time Domain (FDTD) simulation for has been performed. It would be worth mentioning here that the effective-index approach along with a 2D FDTD (as in Huang et al. (1991)) have been adopted here to keep the computational complexity moderate. The electric field distribution of a continuous wave, of wavelength 1550 nm (corresponding to the lattice constant 450 nm and normalized frequency 0.29), travelling through the structure has been shown in Fig. 1b. It can be seen from the figure that the wave initially travels through the W1 port in its fundamental mode. However, after entering the W3 section, it originates higher order modes, which interfere as the wave progresses. The modal interference finally generates a phase-reversed self-image after travelling some distance, and the same is collected at the output port. This phase-reversal is wavelength independent for a large wavelength-window, and this independency can be justified through the modal analysis on the W3 waveguide. In order to arrive to this justification, dispersion characteristic of the W3 waveguide has been calculated by employing the Plane Wave Expansion method. So has been plotted in Fig. 1c, which shows that the W3 waveguide supports three propagation bands within the band gap span of the complete crystal lattice (that ranges from the wavelength 1475 nm to 1570 nm). Therefore, the mode of the wave travelling through the W1 waveguide, after entering the W3 MMI section, gets split up into the three available modes of the W3 waveguide. Out of these three modes, the combination of the fundamental and the first mode generates a beating pattern that repeats within a propagation length of $2\pi/(\beta_1-\beta_0)$, where the β_0 and the β_1 are the propagation constants of the fundamental and the first mode respectively (Soldano and Pennings 1995). Hence, the first mode of the W3 MMI accumulates a π phase-shift with respect to the fundamental mode after travelling the distance $L_\pi = \pi/(\beta_1-\beta_0)$, as described in Eq. (17) in Soldano and Pennings (1995). Now, as can be seen in the Fig. 1c, the fundamental and the first propagation bands of the proposed W3 MMI runs almost parallel along the k-vector, which is the propagation constant normalized with respect to $2\pi/a$. This phenomenon makes the difference of β_1 and β_0 constant over a span of wavelengths. Hence, the length required by the wavelengths in this span for accumulating the π phase-shift with respect to the fundamental mode remains almost same. This length then can be calculated from the normalized wavevectors of the fundamental and the first modes of any arbitrary wavelength within this span. These normalized wavevectors for the wavelength a/0.29 are found from the Fig. 1c as 0.201 and 0.268 respectively, which corresponds to the L_π as 7.46a. Therefore, it can be summarized from the above discussion that a 7-period long W3 PhC waveguide would accumulate an approximately π phase-shift compared to the wave travelling in a W1 waveguide of same length. This statement can be verified by

the Eq. 17 in Soldano and Pennings (1995), which is reproduced here for the convenience of the reader.

$$exp\left[j\frac{m(m+2)\pi}{3L_\pi}L\right] = (-1)^m, \textit{where } m \textit{ is the mode number},$$
$$\textit{and } L \textit{ is the length of the Interferometric section.}$$

The same can also be visualized from the electric field distributions of two parallel W1 waveguides—one without and the other with a 7-period long W3 section, as shown in Fig. 1b. Figure 1d shows the magnitude of the Poynting vector inside the W3 MMI section, which shows that the energy of the fundamental mode initially gets transferred to its two-fold images (Soldano and Pennings 1995) and again combines into a single (phase-shifted) image after length of 7 periods. Moreover, and most noticeably, this phase-shift is expected to be wavelength independent for a large span of wavelengths where the slopes of the fundamental and the first propagation bands of the W3 waveguide remains same.

Now, in order to test the same, a Y-junction interferometer is designed, as shown in Fig. 2a, where the configurations of the input arms (AB and CD) are taken the same as considered in the Fig. 1d. To form the Y-junction, the AB and CD are respectively connected to the W1 waveguides BO and DO, which approach to each other by making 60-degree bends with the input arms. The power delivery through these bends is improved by increasing the radius of their corner holes to 3r, as described in Soldano and Pennings (1995). Moreover, radius of the corner hole at the Y-junction (denoted as 'O') is also taken as 1.6r, to provide the maximum power transfer to the output port (OP) in the case of constructive interference at the junction. Thereafter, both the arms of the interferometer are excited by same-amplitude continuous waves of wavelength 1550 nm. The corresponding electric field distribution within the interferometer and the time evolving graph of power at the output port are shown in the Fig. 2b and c respectively. These figures evidently depict a destructive interference at the Y-junction, which is due to the π phase-shift introduced by the W3 MMI section at the lower arm. To become over-sanguine on this conclusion, the inputs are launched with an initial π phase-difference, and the electric field distribution within the structure along with the time evolving output power are produced in Fig. 2d and e respectively. These figures validate the conclusion by showing the predicted constructive interference at the Y-junction. Also, a study on variation of the output power for a variation in the relative phase difference of the input waves has been performed and the outcome is shown in Fig. 2f. The figure shows that 90% of the input power gets transferred to the output while the initial phase-difference of the waves is kept as π. On the other hand, only 1% of the input power is obtained at the output if the phases of the input waves are the same.

2.2 Design and analysis of a 1:2 decoder

This subsection proposes a design of a Boolean logic 1:2 decoder utilizing the wavelength insensitive phase-shifter proposed in the last sub-section. The design of the decoder, as shown in Fig. 3, can be considered as an extension of the Y-junction interferometer shown in the Fig. 2a. The amendments are done at point B, where another W1 waveguide (BQ) at 60 degree of the AB is attached to form a Y-junction splitter at this point. The BQ is terminated to the other output port (Output-1), named QR, which is a W1 waveguide constructed

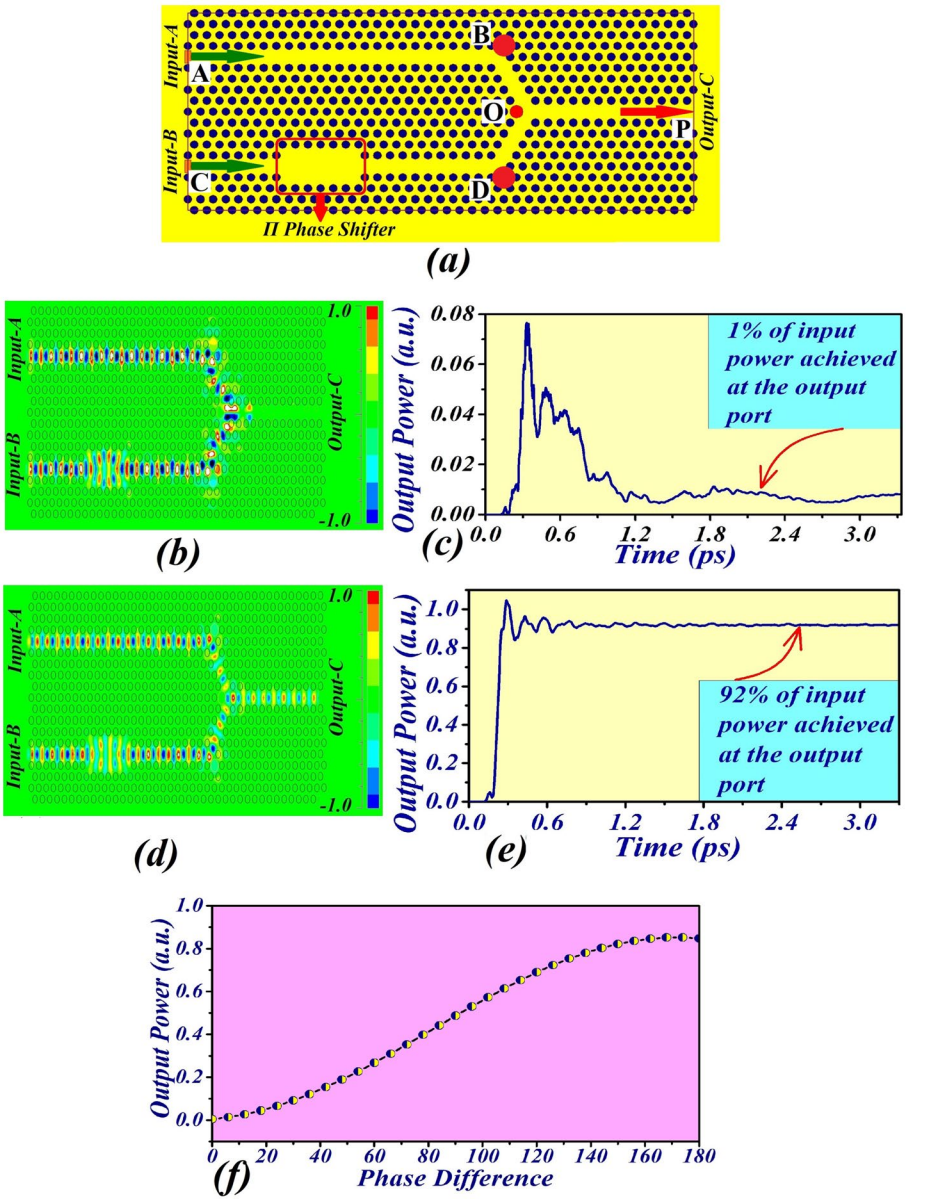

Fig. 2 **a** Physical layout of the interferometer **b** field propagation and **c** output power when inputs are in phase **d** field propagation and **e** output power when inputs are out of phase **f** output Vs. phase changing input graph

in parallel to the AB. It may be noted that the radii of the corner holes at the bending point Q and the Y-junction of B are considered as 3r and 1.6r respectively, based on their heuristic optimization to maximize the output power at the high logic state.

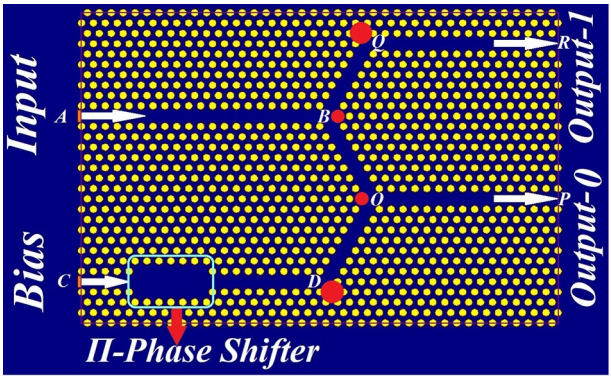

Fig. 3 Physical layout of 1:2 all optical decoder

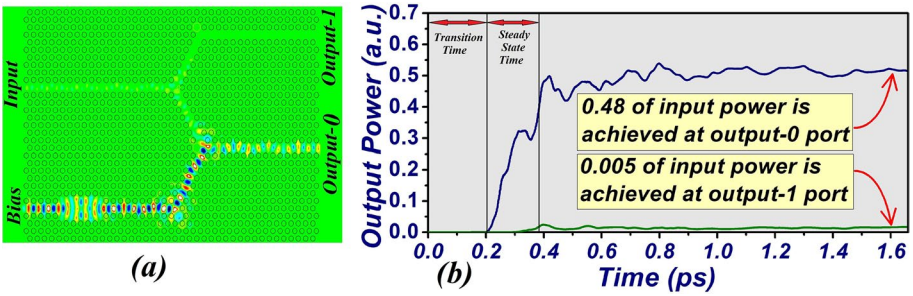

Fig. 4 **a** Field propagation and **b** output power for input logic ZERO

Operation of the device is described as follows. The input port-C is given a continuous wave (CW) excitation at the wavelength 1550 nm. This port is treated as the 'Bias' port and its excitation is considered to be on throughout the operation. The port-A here acts as the 'Input' of the Decoder.

Input at Logic-0: Once the Input is off, i.e., Logic-0, the majority of the optical power of the Bias gets transferred to the output port C (termed as Output-0), as its propagation is not diminished by other waves. Therefore, the Output-0 shows the Logic-1 state at Logic-0 Input. The electric field distribution of this state is shown in the Fig. 4a, which clearly depicts the transfer of maximum energy from the Bias to the Output-0. It also shows that the Output-1 receives only a small amount of Bias power and, hence, can be considered as Logic-0 at this state of the Input. Now, in order to obtain the ratio of the energy transfer of the Bias to both the outputs, the temporal variation of the optical powers at the outputs for this particular state has been recorded and shown in the Fig. 4b. It shows that, at the steady state, 96% of the Bias power gets transferred to the Output-0; whereas so for the Output-1 is merely 1%. The rest of the energy gets scattered at different bends of the PhC waveguide.

Input at Logic-1: On the other hand, the scenario gets changed when the input (port-A) is excited with a CW light of the same phase and wavelength but with twice the power of the Bias (considered as the Logic-1 at input). This is because, at first, the input power gets split up in almost two equal halves at the Y-junction splitter 'B'. One half of this power propagates trough the arm

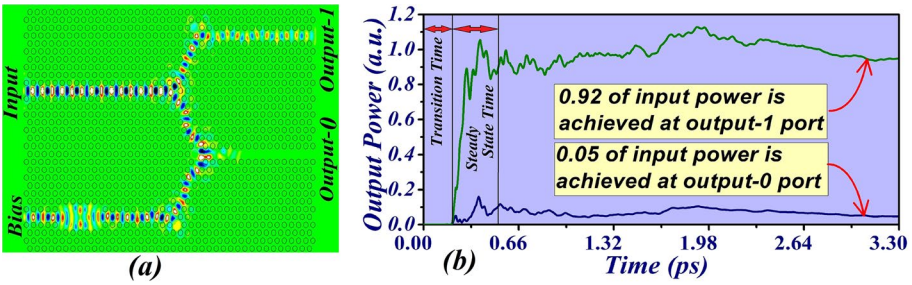

Fig. 5 **a** Field propagation and **b** output power for input logic ONE

Table 1 Truth table of the 1-to-2 line decoder

Bias	Input	Output-0	Output-1
0.5 P_i	0	0.48 P_i	0.005 P_i
0.5 P_i	1	0.05 P_i	0.92 P_i

P_i is the input power

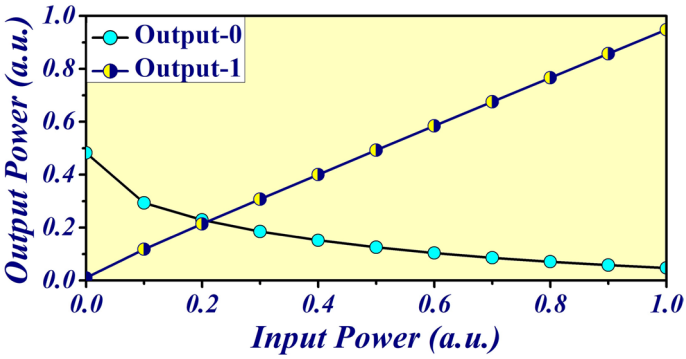

Fig. 6 Output powers for input power variation

BO and meets with the input power in destructive interference at the Y-junction 'O', as the Bias gets π phase shifted by the MMI phase shifter integrated in it. Due to this destructive interference, the Output-0 is fed with almost zero optical power and depicts a Logic-0 state. However, the other half of the Input power propagates to the Output-1 and shows the Logic-1 state. The same phenomenon can be observed from the electric field distribution of wave propagation in this state, which is shown in Fig. 5a. However, the measurement of optical power in this state can be obtained from the temporal variation of the optical powers at the output ports, as shown in Fig. 5b. The figure shows that the Output-1 and Output-0 respectively receives 95% and 5% of the Input power (i.e., 190% and 10% of the Bias power) at this logic state. Therefore, it can be said, when the Input is at Logic-1, the Output-0 is at Logic-0 and the Output-1 is at Logic-1. The truth table of the proposed 1:2 logic decoder has been shown in Table 1, which exhibits a successful decoding operation. The contrast ratios of the Output- 1 and 0 are obtained as 22.6 dB and 9.8 dB respectively, which are reasonably sound for their applications in PICs. The contrast

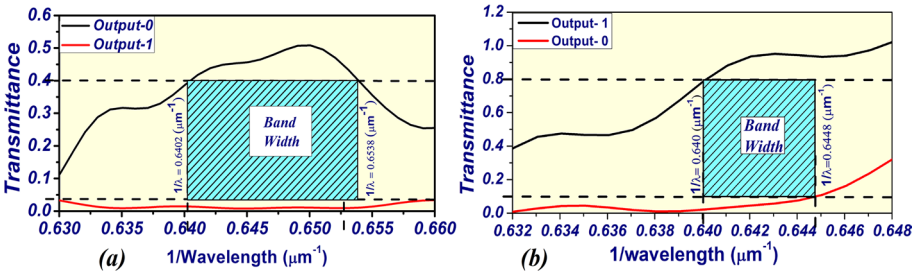

Fig. 7 Transmittance of decoder **a** at zero input condition **b** at one input condition

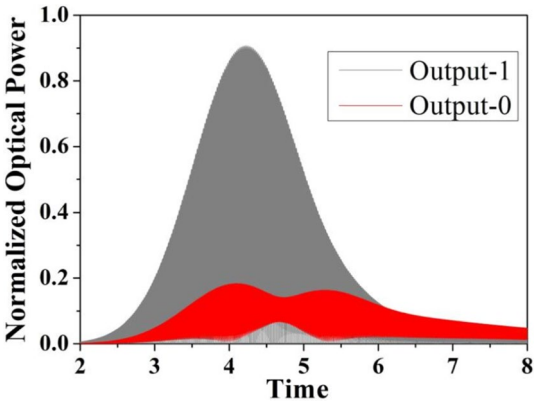

Fig. 8 Temporal evolutions of Output-0 and Output-1 when both Input and Bias are excited with a pulse

ratio is the ratio of optical power at the output port when it is in the state of logic '1' to that of logic '0'. It can be mathematically expressed as follows (Tang et al. 2014):

$$\mathrm{CR} = 10 \log_{10} \left(\mathrm{P}_1 / \mathrm{P}_0 \right),$$

where P_1 is the optical power at the output port for logic '1', and P_0 represents the optical power at the output port for logic '0'. The only demerit of the decoder is that the power at the output ports at the Logic-1 is half of the Input port at the same state. This demerit may be shorted out by using an amplifier at the output stage.

Further, the variations of the power at output ports with that of the Input port have also been studied, and the same have been depicted pictorially in Fig. 6. The figure shows a linear dependency of the power of Output-1 with the power of the Input, which is due to the power splitting at the Y-junction 'B'. On the contrary, the power at the Output-0 decays exponentially with the increase in power at the Input. This is because of the destructive interference at the Y-junction 'O', which has a nonlinear dependency with the power of the interfering waves.

Additionally, transmittances of the output ports of the decoder have been evaluated for both the Logic 0 and Logic 1 states of the Input. Figure 7a and b depict these transmittances for Logic 0 and Logic 1 input states. The powers for the Logic-1 and Logic-0 states at the output are considered to be $\geq 80\%$ and $\leq 10\%$ of the Input (or of the Bias if the Input is zero). In accordance with these logic definitions, Fig. 7a shows that the Output-0 has a

large operating bandwidth, of the order of 4.1 THz. On the other hand, as per Fig. 7b, the Output-1 has a comparatively smaller bandwidth, i.e., ~ 1.44 THz. However, the band for Logic-0 covers the complete band for Logic-1, and hence the device can be said to have a bandwidth of 1.44 THz.

Finally, the decoder operation has been tested under pulsating Input and Bias. The temporal variation of the output ports has been shown in Fig. 8. Figure 8 shows the temporal evaluation of the pulse when both the Input and Bias is excited with a 1 ps pulse. Unlike other logic devices operating in linear optical regime, the figures show that the proposed decoder is able to sustain its operation under time-varying input. Usually, an interference-based device is unable to stick with the desired interference phase for the whole operating band, as the phases of the waves are dependent on their wavelength. However, due to the involvement of wavelength dependent MMI phase shifter within it, the proposed decoder is able to produce the desired destructive interference to the whole band of the temporal pulse. Hence, the device is seen to operate with a pulsating input.

2.3 Fabrication tolerance

Standard CMOS fabrication process like—E-beam Lithography followed by a Reactive Ion Etching is generally used to fabricate a PhC structure. Now, during the fabrication process small deviation in the size of holes may occur from the desired ones because of several instrumental, environmental or random errors, like—mechanical vibration and electrical fluctuation. Therefore, the study of the effect of such deviations in hole-sizes of the proposed structure is essential, as it can hamper the device performance. Therefore, a study on the effect of randomly varied hole-size has been done. To do so, two sets of imperfect structures are made by limiting the deviations up to 10 nm and 20 nm respectively. In each set, 10 similar structures have been made by allowing the radii of the holes to deviate randomly from their ideal value. The device performance as a decoder has been evaluated iteratively for each of these structures. The results for both the input logic combinations for these simulations are recorded, and expressed as a box-plot in Fig. 9. The graph shows that the deviation in output power for both the logic combinations are very small for a random deviation limited within 10 nm. Although the deviation in the port powers for Logic-1 input state is found larger when the random deviations is allowed to 20 nm, the output can still be accepted in several applications. Therefore, it can be stated that the device performance is significantly tolerant up to 20 nm of fabrication imperfections.

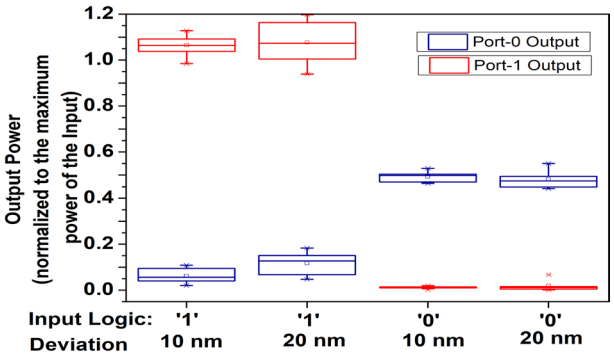

Fig. 9 Box Plot for assessing fabrication tolerance

2.4 Response time and data rate

The response time and data rate of the proposed decoder have been evaluated by analyzing the time-evolving powers of different output ports, as depicted in Figs. 4b and 5b. The response time (Rani et al. 2016) of a device comprises the transition time (Ttr) and the steady-state time (Tss). Ttr represents the duration it takes for a signal to reach 1% of its steady-state power at the desired output port. Conversely, Tss corresponds to the time required for a signal to transition from 1 to 90% of its steady-state output power. Tss is particularly crucial in calculating the bit rate at any given output port. For instance, the Tss at output-0 was measured to be approximately 0.17 ps from its time-evolving graph, i.e., Fig. 4b. Additionally, the falling time is expected to be equal to Tss due to the linear optical operation of the device. Consequently, the width of the narrowest pulse, which is the sum of the rise time and fall time, becomes 2xTss, approximately 0.34 ps. This results in a channel bandwidth of $1/(2 \times \text{Tss})$, i.e., 2.9412 THz. Assuming a return-to-zero (RZ) system, where the bit rate corresponds to half of the bandwidth, the system's bit rate is 1.47 Tb/s. Alternatively, the same channel can provide a higher bit rate in a non-return-to-zero (NRZ) system. Similarly, Tss, bandwidth, and bit rate for output-1 were also calculated using the aforementioned method, as summarized in Table 2.

2.5 Comparative analysis of optical decoder

The decoder's operational principle discussed in this study relies on linear optical phenomena. As indicated in Table 3, a comparative analysis of existing decoders described in the literature reveals that they predominantly operate using the non-linear properties of optics. Table 3 exhibits all the works except one presented in this paper, which utilize the non-linear optical properties of materials. Consequently, the decoders require a threshold optical power for their operation, posing a notable limitation that hinders their practical implementation. Furthermore, it is worth noting from the table below that all the decoders, except for the one presented in this work, have a larger footprint size. This highlights the suitability of this decoder for compact integration in Photonic Integrated Circuits (PICs). Furthermore, the contrast ratio at the ports of the decoder described in this study is superior to that of the other decoders listed in the table. This feature facilitates the reduction of bit-error-rate in communication channels. Consequently, the comparative analysis table underscores the substantial potential of the decoder presented in this work to achieve high data rates and low bit-error-rates without being limited by a threshold optical power.

Table 2 Transition time, steady-state time and bit rate of optical decoder

Output port	Transition time (ps)	Steady State time (ps)	Bit rate (Tb/s) RZ 1 HZ = 0.5 (bits/s)	Bit rate (Tb/s) NRZ 1 HZ = 1 (bits/s)
Output-0	0.21 ps	0.17 ps	1.47 Tbps	2.94 Tbps
Output-1	0.2 ps	0.31 ps	0.81 Tbps	1.62 Tbps

Table 3 Comparative analysis of all-optical logic decoder

Ref	Design platform	Operating principle	Threshold power	Footprint area	Contrast ratio	Data rate/bandwidth/switching frequency	Response time
Moniema (2015)	Rods-in-air	Nonlinear ring resonator	100mW/μm^2	1520 μm^2	–	200 GHz (Switching frequency)	–
Mehdizadeh et al. (2018)	Rods-in-air	Nonlinear ring resonator	50 W/μm^2	581 μm^2	–	10 GHz (Switching frequency)	–
Askarian (2021)	Rods-in-air	Nonlinear ring resonator	20 W/μm^2	420 μm^2	7.73 dB	500 Gbps (Data rate)	2 ps
Alipour-Banaei et al. (2015)	Rods-in-air	Nonlinear ring resonator	1 kW/μm^2	436 μm^2	–	–	–
Khosravi and Zavvari (2018)	Rods-in-air	Nonlinear ring resonator	1 KW/μm^2	309 μm^2	–	–	–
Maleki et al. (2019)	Rods-in-air	Nonlinear cavity	10 mW/μm^2	90 μm^2	–	–	1.9 ps
Salimzadeh and Alipour-Banaei (2018)	Rods-in-air	Nonlinear ring resonator	–	2632 μm^2	–	–	6 ps
Mondal et al. (2018b)	Rods-in-air	Linear optics	Nil	234 μm^2	11.3 dB	625 Gbps	0.77 ps
Mehdizadeh et al. (2016)	Rods-in-air	Nonlinear ring resonator	2 KW/μm^2	1514 μm^2	–	–	–
Mehdizadeh et al. (2017)	Rods-in-air	Nonlinear cavity	20 W/μm^2	2373 μm^2	–	2 GHZ	–
This Work	Holes-in-slab	Linear optics	–	243 μm^2	20 dB	2 Tbps	0.51 ps

3 Conclusion

This work proposes the design of a PhC-based all-optical 1-to-2-line decoder that operates on the principle of optical interference. The phase difference of the interfering beams is usually dependent on their wavelengths, as the wave vectors are wavelength dependent. This narrows down the operating bands of such interference-based devices. In order to encounter the same, this work first proposes a PhC MMI-based design for a π-phase-shifter, which is insensitive to the variation of wavelength within a large span. The design principle of the phase-shifter is based on the analytical outcome of the dispersion diagram of the MMI section. FDTD simulation has been used to verify the wavelength insensitivity of the phase shifter. Thereafter, this phase-shifter is used in the design of the 1-to-2-line optical decoder to enable its operation for a large wavelength band. FDTD simulations have been performed to establish the operation of the device under different possible logic states. Finally, the decoding operation is tested under pulsating inputs using pulses of width 1 ps, corresponding to a bit rate of 1 THz. The device is seen to operate successfully under the pulsating regime, which is a significant achievement with respect to devices operating in the linear optical regime. The transmittance analyses have also confirmed that the device is able to operate up to a bit rate of 1.44 THz, considering $\geq 80\%$ transmission at logic 1 and $\leq 10\%$ at logic 0. With such a remarkable performance, the proposed silicon PhC-based all-optical logic decoder is expected to find numerous applications in PICs. Also, the MMI-based π-phase-shifter can be used to design other photonic devices as well.

Acknowledgements Not applicable

Author contribution Kamanashis Goswami, Haraprasad Mondal and Mrinal Sen have equally contributed toward Simulation of the work, preparing pictures, graphs and writing of the manuscript. All the authors have read and approved the final manuscript.

Funding The authors did not receive fund from any organization for the submitted work.

Data availability We don't have any supplementary dataset along with the manuscript.

Declarations

Competing interests The authors have no competing interests to declare that are relevant to the content of this article.

Ethics approval We declare that the manuscript entitled "Design of 1-to-2-line all-optical decoder based on MMI phase shifter" is original, has not been fully or partly published before, and is not currently being considered for publication elsewhere. Moreover, we confirm that no figures and graphs have been reproduced in this manuscript. We further confirm that the order of authors listed in the manuscript has been approved by all of us.

Consent to participate Not applicable.

Consent for publication Not applicable.

References

Alipore, A., Farmani, A., Mir, A.: High sensitivity and tuneable nanoscale sensor based on plasmon-induced transparency in plasmonic meta surface. IEEE Sens. J. **18**, 7047–7054 (2018)

Alipour-Banaei, H., Mehdizadeh, F., Serajmohammadi, S., Kashtiban, M.H.: A 2*4 all optical decoder switch based on photonic crystal ring resonators. J. Mod. Opt. **62**(6), 430–434 (2015)

Askarian, A.: Design and analysis of all optical 2 × 4 decoder based on kerr effect and beams interference procedure. Opt. Quantum Electron. **53**, 291 (2021). https://doi.org/10.1007/s11082-021-02987-9

Baqir, M.A., Farmani, A., Fatima, T., Raza, M.R., Shaukat, S.F., Mir, A.: Nanoscale, tuneable, and highly sensitive biosensor utilizing hyperbolic metamaterials in the near-infrared range. Appl. Opt. **57**, 9447–9454 (2018)

Cabezón, M., Sotelo, F., Altabás, J.A., Garcés, J.I., Villafranca, A.: Integrated all-optical 2-bit decoder based on semiconductor optical amplifiers. In: 2014 16th International conference on transparent optical networks (ICTON) (2014), p. 1–4. https://doi.org/10.1109/ICTON.2014.6876637

Chen, Z., Li, Z., Li, B.: A 2-to-4 decoder switch in SiGe/Si multimode interference. Opt. Express **14**, 2671–2678 (2006)

Chung, S., Lee, C.-K., Kim, Y., Lim, Y., Seo, S.W., Lee, B.: A simply tunable optical CDMA encoder/decoder for two-dimensional cyclic permutable codes. In: 2006 Optical fiber communication conference and the national fiber optic engineers conference (2006), p. 3. https://doi.org/10.1109/OFC.2006.215545

Fu, Y., Hu, X., Gong, Q.: Silicon photonic crystal all-optical logic gates. Phys. Lett. A **377**(3), 329–333 (2013)

Gogoi, D., Das, K., Mondal, H.P., Talukdar, P., Hussain, K.: Design of ultra-compact 3-channel wavelength de-multiplexer based on photonic crystal. In: IEEE international conference on automatic control and dynamic optimization technique (ICACDOT-2016), I2IT, Pune, Maharashtra (2016)

Goswami, K., Mondal, H.P., Sen, M.: A review on all-optical logic adder: heading towards next-generation processor. Opt. Commun. **483**, 126668 (2020a)

Goswami, K., Mondal, H., Sen, M.: Optimized design of 60° bend in optical waveguide for efficient power transfer. In: Advances in Communication, Devices and Networking Lecture Notes in Electrical Engineering. Springer, New York (2020b)

Goswami, K., Mondal, H.P., Das, P., Thakuria, K.: Realization of ultra-compact all-optical logic AND gate based on photonic crystal waveguide". In: Advances in Communication, Devices and Networking, pp. 61–68. LNEE Springer, Singapore (2022)

Goswami, K., Mondal, H., Sen, M.: Design and analysis of all-optical isolator based on linear photonic crystal. Braz. J. Phys. **52**(78), 1–10 (2022a)

Goswami, K., Mondal, H., Sen, M.: Optimized design of multiple bends for maximum power transfer in optical waveguide. Optik **265**, 169448 (2022b)

https://mpb.readthedocs.io/en/latest/Introduction/. Accessed 12 May 2023

https://www.synopsys.com/photonic-solutions/rsoft-photonic-device-tools/passive-device-fullwave.html. Accessed 12 May 2023

Huang, W., Chu, S., Chaudhuri, S.: A semi-vectorial finite difference timedomain method (optical guided structure simulation). IEEE Photonic Technol. Lett. **3**, 803–806 (1991)

Jiu-Sheng, Li., Han, L., Le, Z.: Compact four-channel terahertz demultiplexer based on directional coupling photonic crystal. Opt. Commun. **350**, 248–251 (2015)

Joannopoulos, J.D., Johnson, S.G., Winn, J.N., Meade, R.D.: Photonic Crystals: Molding the Flow of Light, 2nd edn. Princeton University Press, Princeton (2008)

Johnson, S.G., Joannopoulos, J.D.: Block-iterative frequency domain methods for Maxwell"s equations in a plane wave basis. Opt. Express **8**, 173–190 (2001)

Johnson, S.G., Fan, S., Villeneuve, P.R., Joannopoulos, J.D.: Guided modes in photonic crystal slabs. Phys. Rev. B **60**(8), 5751–5758 (1999)

Khosravi, S., Zavvari, M.: Design and analysis of integrated all-optical 2 × 4 decoder based on 2D photonic crystals. Photon. Netw. Commun. **35**, 122–128 (2018)

Kim, S.: Cyclic optical encoders/decoders for compact optical CDMA networks. IEEE Photonics Technol. Lett. **12**(4), 428–430 (2000). https://doi.org/10.1109/68.839041

Lee, W, Kim, B.K., Park, H., Kim, K.: Tunable optical CDMA encoder/decoder based on modified PN code using FBG array. In: 2006 optical fiber communication conference and the national fiber optic engineers conference (2006), p. 3. https://doi.org/10.1109/OFC.2006.215536

Lin, W.-P., Hsu, Y.-F., Kuo, H.-L.: Design of optical NOR logic gates using two dimension photonic crystals. J. Mod. Phys. **2**(3), 144–147 (2013)

Liu, W., Yang, D., Shen, G., Tian, H., Ji, Y.: Design of ultra-compact alloptical XOR, XNOR, NAND and OR gates using photonic crystal multimode interference waveguides. Opt. Laser Technol. **50**, 55–64 (2013)

Maleki, M.J., Soroosh, M., Mir, A.: Improving the performance of 2-to-4 optical decoders based on photonic crystal structures. Crystals **9**(12), 635–643 (2019)

Mehdizadeh, F., Soroosh, M., Alipour-Banaei, H.: A novel proposal for optical decoder switch based on photonic crystal ring resonators. Opt. Quantum Electron. **48**, 20–29 (2016)
Mehdizadeh, F., Alipour-Banaei, H., Serajmohammadi, S.: Study the role of non-linear resonant cavities in photonic crystal-based decoder switches. J. Mod. Opt. **64**, 1233–1239 (2017)
Mehdizadeh, F., Banaei, H.A., Serajmohammadi, S.: Design and simulation of all optical decoder based on nonlinear PhCRRs. Optik Int. J. Light Electron. Opt. **156**, 701–706 (2018)
Mondal, H., Sen, M., Prakash, C., Goswami, K., Sarma, C.: Impedance matching theory to design an all optical AND gate. IET Optoelectron. **12**(5), 244–248 (2018b)
Mondal, H., Sen, M., Goswami, K.: Design and analysis of a 0.9Tb/s 6-channel WDM filter based on photonic crystal waveguides. J. Opt. Soc. Am. B **36**, 3181–3188 (2019). https://doi.org/10.1364/JOSAB.36.003181
Mondal, H., Sen, M., Goswami, K.: Design and analysis of all-optical 1 to 2 line decoder based on linear photonic crystal. IET Optoelectron. **13**(4), 191–195 (2019)
Mondal, H.P., Goswami, K., Sen, M., Khan, W.R.: Design and analysis of all-optical logic NOR gate based on linear optics. Opt. Quantum Electron. **54**, 272 (2022). https://doi.org/10.1007/s11082-022-03624-9
Mondal, H. P., Chanda, S., Sen, M., Datta, T.: All-optical AND gate based on silicon photonic crystal. In: IEEE international conference on microwave and photonics, Indian School of Mines, Dhanbad, Jharkhand (2015)
Mondal, H.P., Chanda, S., Gogoi, P.: Realization of all-optical logic AND gate using dual ring resonator. In:IEEE international conference on automatic control and dynamic optimization technique (ICACDOT-2016), I2IT, Pune, Maharashtra (2016)
Mondal, H.P., Goswami, K., Sen, M., Prakash, C.: An all-optical ultra-compact 4-channel wavelength demultiplexer. In: IEEE international conference on microwave and photonics, Indian School of Mines, Dhanbad, Jharkhand (2018a)
Moniema, A.T.: All optical active high decoder using integrated 2D square lattice photonic crystals. J. Mod. Opt. **62**(19), 1643–1649 (2015)
Prakash, C., Sen, M., Mondal, H., Goswami, K.: Design and optimization of a TE-pass polarization filter based on a slotted photonic crystal waveguide. J. Opt. Soc. Am. B **35**(8), 1791–1798 (2018a)
Prakash, C., Mondal, H., Goswami, K., Sen, M.: Investigation of optimum position of interface between strip waveguide and PhC Slot waveguide for maximum power coupling. In: IEEE III international conference on microwave and photonics (ICMAP) 2018b, Indian School of Mines, Dhanbad, Jharkhand, India (2018b). https://doi.org/10.1109/ICMAP.2018.8354622
Rani, P., Kalra, Y., Sinha, R.K.: Design and analysis of polarization independent all-optical logic gates in silicon-on-insulator photonic crystal. Opt. Commun. **374**, 148–215 (2016)
Rostami, A.: Piecewise linear integrated optical device as an optical isolator using two-port nonlinear ring resonators. Opt. Laser Technol. **39**(5), 1059–1065 (2007)
Sahoo, P.K., Joseph, J.: Optical diode using nonlinear polystyrene ring resonators in two-dimensional photonic crystal structure. Appl. Opt. **52**, 8252–8257 (2013)
Salimzadeh, S., Alipour-Banaei, H.A.: A novel proposal for all optical 3 to 8-decoder based on nonlinear ring resonators. J. Mod. Opt. **65**, 2017–2024 (2018)
Serajmohammadi, S., Alipour-Banaei, H., Mehdizadeh, F.: A novel proposal for all optical 1-bit comparator using nonlinear PhCRRs. Photonics Nanostruct. Fundam. Appl. **34**, 19–23 (2019)
Sharma, A., Goswami, K., Mondal, H.P., Datta, T., Sen, M.: A review on photonic crystal based all-optical logic decoder: linear and nonlinear perspectives. Opt. Quantum Electron. **54**, 90 (2022). https://doi.org/10.1007/s11082-021-03473-y
Soldano, L.B., Pennings, E.C.M.: Optical multi-mode interference devices based on self-imaging: principles and applications. J. Lightwave Technol. **13**(4), 615–627 (1995)
Sukhoivanov, I.A., Guryev, I.V.: Photonic Crystals: Physics and Practical Modeling. Springer, Germany (2009)
Tang, C., Dou, X., Lin, Y., Yin, H., Bin, Wu., Zhao, Q.: Design of all-optical logic gates avoiding external phase shifters in a two-dimensional photonic crystal based on multi-mode interference for BPSK signals. Opt. Commun. **316**, 49–55 (2014)
Xie, J., Niu, X., Hu, X., Wang, F., Chai, Z., Yang, H., Gong, Q.: Ultracompact all-optical full-adder and half-adder based on nonlinear plasmonic nanocavities. Nanophotonic **6**, 1161–1173 (2017)
Yablonovitch, E.: Inhibited spontaneous emission in solid-state physics and electronics. Phys. Rev. Lett. **58**, 2059–2062 (1987)
Zhang, Y., Zhang, Y., Li, B.: Optical switches and logic gates based on self-collimated beams in two-dimensional photonic crystals. Opt. Express **15**(15), 9287–9292 (2007)
Zhao, T., Asghari, M., Mehdizadeh, F.: An all-optical digital 2-to-1 multiplexer using photonic crystal based nonlinear ring resonators. J. Electron. Mater. **48**, 2482–2486 (2019)

Zhu, Q., Li, B.: Photonic crystal waveguide-based Mach-Zehnder demultiplexer. Appl. Opt. **45**, 8870–8873 (2006)